



RESEARCH LETTER

10.1002/2014GL060848

Key Points:

- Precursors in shear wave amplitudes occur prior to slip along a discontinuity
- Precursors are linked to changes in the stiffness of a discontinuity

Correspondence to:

A. Hedayat,
hedayata@ipfw.edu

Citation:

Hedayat, A., L. J. Pyrak-Nolte, and A. Bobet (2014), Precursors to the shear failure of rock discontinuities, *Geophys. Res. Lett.*, *41*, 5467–5475, doi:10.1002/2014GL060848.

Received 13 JUN 2014

Accepted 26 JUL 2014

Accepted article online 29 JUL 2014

Published online 12 AUG 2014

Precursors to the shear failure of rock discontinuities

Ahmadreza Hedayat¹, Laura J. Pyrak-Nolte², and Antonio Bobet³

¹Civil Engineering Program, Department of Engineering, Indiana University-Purdue University, Fort Wayne, Indiana, USA, ²Department of Physics, Department of Earth and Atmospheric Sciences, School of Civil Engineering, Purdue University, West Lafayette, Indiana, USA, ³School of Civil Engineering, Purdue University, West Lafayette, Indiana, USA

Abstract Active geophysical monitoring of potential failure along mechanical discontinuities in rock requires identification of precursory signatures to failure in geophysical signals. Active ultrasonic monitoring of shear failure along frictional discontinuities was performed to determine the signatures of potential failure. An instrumented direct shear apparatus was used to apply a constant shearing rate to a discontinuity that was held under a constant normal stress. Transmitted and reflected compressional and shear waves were recorded during the shearing process. Ultrasonic precursors were identified as distinct maxima in the amplitude of transmitted shear waves as well as minima in the amplitude of reflected shear waves that occurred well before the peak shear strength of a frictional discontinuity. The precursors are linked to changes in the local shear specific stiffness along the discontinuity, while the discontinuity's macroscopic shear strength continues to increase prior to failure.

1. Introduction

Frictional sliding is widely accepted as the most likely mechanism for shallow earthquakes and has been continuously investigated as a prerequisite to the understanding of earthquake mechanisms [Brace and Byerlee, 1966; Byerlee, 1970, 1978; Brace, 1972; Scholz, 1998; Jaeger et al., 2007].

Laboratory stick-slip studies are the small-scale counterpart of the study of earthquakes [Byerlee and Brace, 1968; Brace, 1972; Scholz et al., 1972; Stesky et al., 1974; Byerlee and Summers, 1975; Johnson and Scholz, 1976; Dieterich, 1978a, 1979; Okubo and Dieterich, 1984; Weeks and Tullis, 1985; Ohnaka and Kuwahara, 1990; Sobolev et al., 1993; Marone, 1998; Scholz, 2002; Johnson et al., 2008; McLaskey et al., 2012]. The prediction of earthquakes triggered by stick-slip events is a fascinating but challenging field of research. Several premonitory phenomena such as changes in acoustic emission (AE) events, velocity, and amplitude [Lockner et al., 1977; Yanagidani et al., 1985; Thompson et al., 2009; Johnson et al., 2013]; electrical resistivity [Lockner and Byerlee, 1986]; the ratio of seismic velocities and seismic wave attenuation [Aggarwal et al., 1973; Lockner et al., 1977; Chen et al., 1993; Kaproth and Marone, 2013]; permeability [Zoback and Byerlee, 1975; Morrow et al., 1981]; Gutenberg-Richter *b* value [Weeks et al., 1978; Meredith et al., 1990]; microslip [Johnson et al., 2013]; and microscopic rearrangement of particles [Nasuno et al., 1997] have been observed in laboratory studies. Although finding a reliable precursor has been elusive [Cicerone et al., 2009], wave propagation methods proved to be among the most promising methods in capturing the stress-dependent behavior of rock discontinuities.

AE is an invaluable tool to evaluate fracturing and microseismic activities during shearing. AE has been successfully used in laboratory experiments to provide insights into deformation processes occurring in intact rocks [Lockner, 1993] and along existing discontinuities [Weeks et al., 1978; Sammonds and Ohnaka, 1998; Yabe et al., 2003; Mair and Hazzard, 2007; Johnson et al., 2008; Thompson et al., 2009; Johnson et al., 2013]; however, it is unclear whether AE events are precursors to slip or the results of slip [Chen et al., 1993; Goebel et al., 2013].

An alternative to AE is active monitoring geophysical methods, in particular, compressional and shear wave propagation, which have the potential to locate discontinuities, assess the state of the stress along discontinuities and provide information about the engineering properties of discontinuities such as stiffness [Pyrak-Nolte et al., 1990; Chen et al., 1993; Pyrak-Nolte, 1996; Hildyard et al., 2005].

2. Experimental Methods

Direct shear experiments were conducted using a direct shear apparatus (shown in Figure 1), consisting of a horizontal loading frame to apply the normal stress on the contact surface and a standard loading machine to

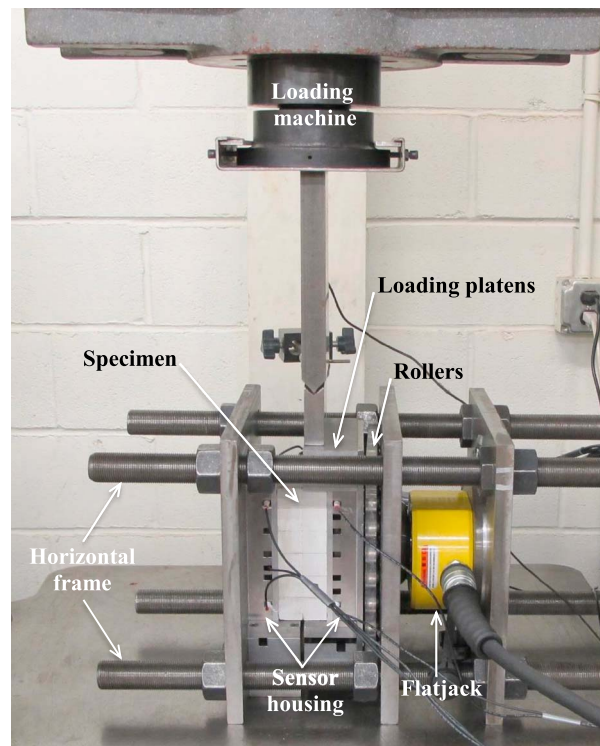


Figure 1. Experimental apparatus. The instrumented direct shear apparatus consisted of a horizontal loading frame to apply the constant normal stress and a conventional loading machine to apply the shear stress at a constant shearing rate. The apparatus allows making precise ultrasonic shear wave measurements during the shear experiments.

apply the shear stress along the contact surface. The horizontal loading frame was composed of a flatjack, loading platens that encased the specimen and sensors, steel rods, rollers, and plates. The flatjack was placed behind the steel plate to apply a normal stress to the loading plates and the specimen. A series of rollers were placed between the loading platen and the steel plate to minimize vertical friction and to ensure that the vertical load was resisted solely by the contact surface between the blocks. The direct shear experiments were conducted under applied normal stress of 1–4 MPa and with the shearing rate of $8 \mu\text{m/s}$. Two linear variable differential transformers (LVDT) placed on top of the specimen recorded the average vertical displacement of the specimen, while the load cell in the loading machine recorded the applied shear load. An electronic feedback loop was used to control the flatjack pressure to maintain the horizontal stress constant, as the Poisson effects could induce horizontal expansion of the specimen during shearing. Compressional and shear wave ultrasonic pulses were transmitted through and reflected off the discontinuity during the direct shear experiments.

An ultrasonic wave measurement system was used to continuously monitor a discontinuity during shear experiments. Two arrays, each with 13 embedded seismic (ultrasonic) transducers, were placed on the sides of the specimen during direct shear testing. The ultrasonic transducers (Panametrics V153RM) were 11 mm diameter cylindrical transducers with a central frequency of 1 MHz. Two pulser-receivers (Panametrics 5077PR) were used to generate square wave pulses with 100 V magnitude with a repetition rate of 5 kHz and a gain of +10 dB. The specimen assembly process was standardized to ensure repeatability of the seismic measurements. The transducers were coupled to the surface of the specimens using oven-baked honey (Beehive Honey) as the coupling medium. A fast LabView-controlled data acquisition system with a sampling rate of 20 million samples/s (or $0.05 \mu\text{s}$ per point) recorded full waveforms in real time. For each transducer, 30 transmitted signals were stacked for each output measurement to increase the signal-to-noise ratio. The total time required for the waveform acquisition through all 13 transducers was 0.5 s (i.e., sampling rate of 2 Hz).

For the frequencies on the order of a Megahertz, the amplitude of the transmitted shear wave is more sensitive to changes of the discontinuity properties than the wave velocity [Pyrak-Nolte *et al.*, 1990; Chen *et al.*, 1993; Johnson *et al.*, 2008].

For the frequencies on the order of a Megahertz, the amplitude of the transmitted shear wave is more sensitive to changes of the discontinuity properties than the wave velocity [Chen *et al.*, 1993; Johnson *et al.*, 2008]. The seismic spectrum in nature may range from 0.01 to 10 Hz [Johnson *et al.*, 2008]. Despite the difference between the laboratory and the frequencies that occur from natural processes, laboratory ultrasonic studies are useful in developing an understanding of physical phenomena that occur in nature.

Digital image correlation (DIC) technique [Pan *et al.*, 2009; Schreier *et al.*, 2009] was used to measure surface displacements during the experiments. DIC is a noncontact and full-field measurement technique that is widely used to investigate deformation and fracture of materials and structures. DIC uses a correlation algorithm to compare digital images of the specimen surface acquired prior and

during deformation [Chu *et al.*, 1985; Pan *et al.*, 2009]. The image taken before deformation is the reference image and is used as the basis for comparison with images taken during deformation or loading. A region of interest (ROI) is defined first within the image, and the ROI is then divided into subsets of images by an evenly spaced grid so that the displacement field can be calculated at the grid points [Pan *et al.*, 2009]. In DIC, subsets of images are tracked between the deformed and the reference image. The reason for choosing a subset rather than a single point is that a square subset provides a matrix of gray scale intensity values with a unique arrangement that makes it identifiable, while a single point with a single gray intensity value may be found in thousands of other points in the image. When the correlation between the reference and the deformed subsets reaches an extremum (i.e., minimum or maximum depending on the type of the correlation criterion), optimal matching is found between the two subsets. The coordinates of the extremum position define the new (displaced) position of the deformed subset. The difference between the new position of the deformed subset and the center of the reference subset yields the displacement vector.

The implementation of the DIC method required the following consecutive steps: (a) specimen preparation, (b) image acquisition, and (c) image correlation using a computer program. To create a unique and random speckle pattern for the purpose of DIC, a textured spray paint was used to coat the specimen surface. A camera and a lens were used to capture the entire surface of the specimen. A Grasshopper (Point Grey) CCD camera with 2448×2048 square pixels was used in combination with a Fujinon lens having a focal length of 75 mm (Model HF75SA-1) with manual control of the aperture, focus, and zoom. Digital images were recorded at the rate of 4 frames/s. The depth of field for the imaging system was ± 1 mm. The image correlation was performed using the software Vic-2D, licensed by Correlated Solutions. The accuracy of the displacement measurement system was $1.87 \mu\text{m}$ [Hedayat, 2013].

3. Results

Direct shear experiments were conducted on discontinuities in two types of materials: gypsum and Indiana limestone. Gypsum has been extensively used as a rock model material in other studies [Einstein and Hirschfeld, 1973; Shen *et al.*, 1995; Bobet and Einstein, 1998].

Gypsum specimens were fabricated in the laboratory and consisted of two prismatic blocks each with dimensions of 152.4 mm long, 127 mm wide, and 50.8 mm thick with fully mated contact surfaces. Gypsum contact surfaces were made by casting gypsum against the base of a mold with different frictional characteristics. Two types of contact surfaces were made: homogeneous and nonhomogeneous. Homogeneous smooth contact surfaces were made by casting gypsum in a mold with a smooth plastic sheet at its base to create a uniform contact. A homogeneous rough surface was created by casting the gypsum against sandpaper with grit #36 ($530 \mu\text{m}$). Nonhomogeneous contact surfaces were made by placing a smooth plastic sheet on one half and sandpaper (grit #36) on the other half of the base of the mold. After the first gypsum block had hardened, the second block was cast against the first one, thus creating a perfectly mated contact surface.

Surface roughness measurements performed on the gypsum specimen contact surfaces showed that the maximum variation in the height of asperities was ± 0.1 and ± 0.4 mm for the smooth and rough surfaces, respectively. Also, direct shear experiments found peak friction angles of 38° (friction, $\mu \sim 0.78$) and 50° ($\mu \sim 1.2$) for the homogeneous smooth and rough specimens, respectively.

Indiana limestone specimens were made by inducing a single tensile fracture in the intact rock. This technique is similar to Brazilian testing or split cylinder method, where two thin rods are placed to opposite sides of the specimen and a compressional load is applied. The maximum variation in the height of asperities on the fractured Indiana limestone surface was ± 3 mm. In comparison with homogeneous rough gypsum contact surfaces, the size of the asperities in limestone was approximately 10 times larger. Direct shear experiments performed on the limestone discontinuities showed a peak friction angle of 61° ($\mu \sim 1.8$).

The normalized peak-to-peak amplitude as a function of shear displacement is shown in Figure 2 for a nonhomogeneous gypsum specimen that was sheared in the direct shear apparatus. The peak-to-peak signal amplitude was normalized with respect to its initial value prior to shear and the displacements are given with respect to the displacement needed to reach the peak shear strength (failure).

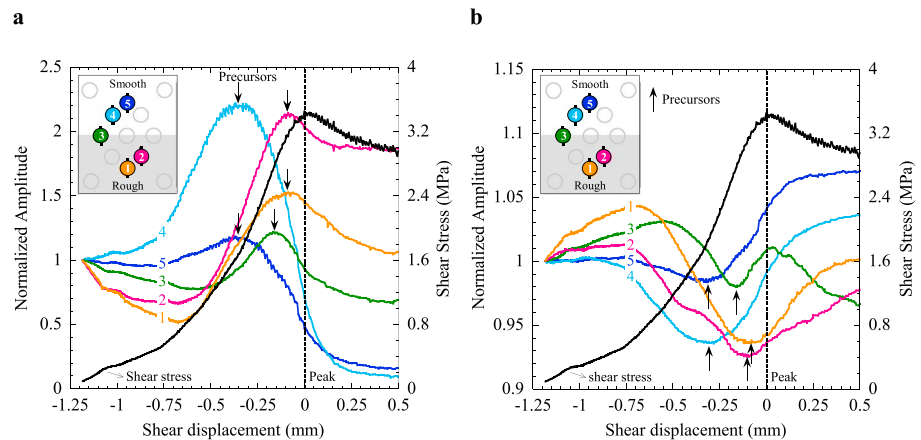


Figure 2. Ultrasonic precursors to the failure of a nonhomogeneous discontinuity subjected to a normal stress of 3 MPa. (a) Transmitted shear wave amplitudes and shear stress displacement. (b) Reflected shear wave amplitudes and shear stress displacement. Inset: Transducer layout used for seismic measurements. The lines on the circles indicate the polarization of the shear waves, which is parallel to the shearing direction for all transducers.

As shown in Figure 2a, after the initial seating deformation of the specimen, from -1.25 mm to -0.75 mm of shear displacement, the shear stress increased rapidly with shear displacement until it reached the peak shear strength of the discontinuity. The amplitude of the transmitted shear waves increased as the shear load was transferred to the specimen (Figure 2a). Distinct maxima in the normalized transmitted shear wave amplitudes occurred prior to the peak shear strength. A maximum in transmitted amplitude was observed in the signals from all of the transducers and was identified as an ultrasonic precursor that indicates impending shear failure of the discontinuity. The maximum in amplitude was followed by a decrease as additional shear displacement occurred along the discontinuity. The decrease in the amplitude was greater for the smooth surface (i.e., transducers on the upper half of the discontinuity) than for the rough surface (i.e., transducers on the lower half of the discontinuity). Figure 2b shows the amplitude of the reflected shear waves measured with the transmitted signals. The amplitude of the reflected signals decreased upon application of the shear load and attained a minimum prior to reaching the peak shear strength. The minimum in the amplitude of the reflected wave corresponded to the maximum of the amplitude of the transmitted waves. After reaching the minimum, the amplitude of the reflected waves increased due to the reduction of the discontinuity's shear specific stiffness.

The data shown in Figure 2 are representative of an extensive experimental study, where over 100 direct shear experiments were performed on discontinuities in gypsum. The main implication of the data is the identification of precursors as significant changes in the transmitted and reflected shear wave amplitudes that occur prior to peak shear strength. The precursors were evaluated as a function of the distance (i.e., shear displacement) between their appearance and the peak shear strength. The discussion here is based on displacement rather than on time to eliminate the effect of loading rate. For a better interpretation of the precursors, negative values are used to denote the magnitude of the shear displacement that remains before reaching the peak shear stress. Thus, the more negative the value, the earlier the precursor.

Figure 3 shows a summary of precursor events observed from direct shear experiments on gypsum. The figure consists of three parts: (a) precursor events observed for homogeneous smooth discontinuities, (b) precursor events observed for homogeneous rough discontinuities, and (c) precursor events observed for nonhomogeneous discontinuities. The precursors to peak shear strength were observed between -0.2 mm and 0 mm for homogeneous smooth discontinuities (Figure 3a), between -0.36 mm and -0.1 mm for homogeneous rough discontinuities (Figure 3b), and between -0.48 mm and -0.2 mm for the nonhomogeneous discontinuities (Figure 3c). Although the magnitude of the displacement may seem to be small in terms of its absolute value, it is a significant fraction of the peak displacement. In fact, precursors appear within the range of 50% to 80% of the peak displacement. The scatter that is observed in Figure 3 shows only the variation in the range of precursors observed for all experiments conducted on the same type of specimen surface.

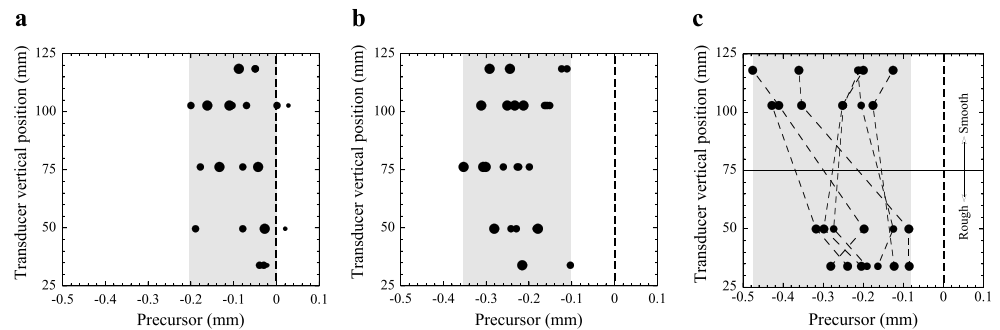


Figure 3. Summary of ultrasonic precursors observed prior to the failure of discontinuities in gypsum. (a) Homogeneous smooth discontinuities. (b) Homogeneous rough discontinuities. (c) Nonhomogeneous discontinuities. The location of the precursors is measured from the bottom of the specimen. The figures contain the results of a series of experiments performed on each type of discontinuity at normal stresses ranging from 1 to 4 MPa. The size of the circles represents the level of applied normal stress. The bigger the circle, the higher the normal stress.

The precursors were detected closer to the macroscopic peak shear strength of the homogeneous smooth discontinuity (Figure 3a) than to the macroscopic shear strength of the homogeneous rough discontinuity (Figure 3b). For specimens with a nonhomogeneous discontinuity, it was observed that the precursors tended to occur first on the smooth surface and later on the rough surface or almost simultaneously along the entire discontinuity. Given that the shear displacement between precursors and failure should be much smaller for a smooth surface (Figure 3a) than for a rough surface (Figure 3b), the data in Figure 3c, from nonhomogeneous discontinuities, suggest that slip occurred first along the smooth surface and later along the rough surface.

The observation that slip occurred first along the smooth (weak) surface and later along the rough (strong) surface is in agreement with previous findings [Martel and Pollard, 1989; Bürgmann and Pollard, 1994; Bruhn and Schultz, 1996; Mutlu and Bobet, 2006], demonstrating that slip along a discontinuity does not occur simultaneously. It starts first along a weak patch and then propagates along the discontinuity. As observed in our experiments, the sequence of the precursors prior to failure indicates a nonuniform distribution of microslip events along the discontinuity.

In the following, we coupled the geophysical measurements with the slip distribution along the nonhomogeneous discontinuity. We used the DIC technique to measure shear displacements along the discontinuity. Slip, defined as the relative shear displacement across a discontinuity, was calculated from the surface displacement data separately for the smooth and rough portions of the discontinuity. The amplitude of the transmitted shear wave from each transducer was normalized with respect to its maximum value during the test. The ultrasonic sensors probe regions of the discontinuity that are within the lobe pattern of the beam. The ultrasonic transducers measure the local changes in the properties of a discontinuity and are then compared with the average slip for the surface over which they are located. A comparison of the ultrasonic measurements with slip is given in Figure 4.

A significant increase in the rate of slip was observed to occur first in the smooth portion of the surface and was concurrent with the precursor from the ultrasonic transducers located in the smooth region. The significant increase in the rate of slip occurred closer to failure for the rough surface than for the smooth surface and was also associated with the corresponding ultrasonic precursor observed at the rough surface. It is clear from the results that the precursor events were associated with an acceleration in the rate of slip along the discontinuity. According to the rate- and state- variable friction law, an increase in the rate of slip is attributable to a reduction in the true contact area [Dieterich, 1978b; Dieterich and Kilgore, 1994]. Rock discontinuities consist of two rough surfaces in partial contact and the true (real) contact area is not the same as the nominal contact area. At a discontinuity between two rock blocks, a seismic wave is transmitted through contact points and reflects from the voids between the points of contact. The intensity of the wave transmitted through the discontinuity is a measure of the elastic specific stiffness of the discontinuity, which is related to the true contact area [Kendall and Tabor, 1971; Schoenberg, 1980; Pyrak-Nolte et al., 1990]. An increase in the true contact area results in an increase in wave transmission across the discontinuity and conversely a decrease in the intensity of the reflected wave. Therefore, precursors, as

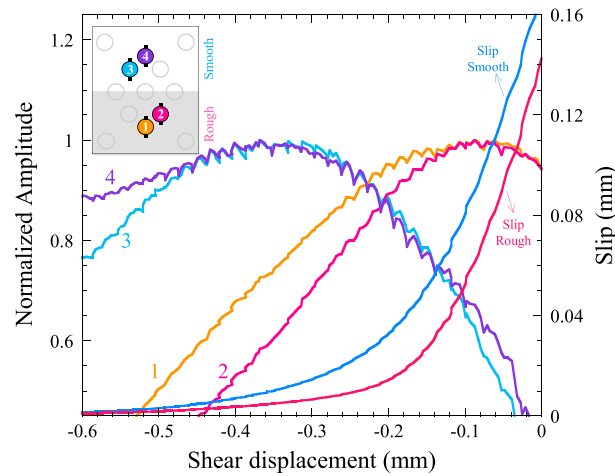


Figure 4. Ultrasonic precursors and slip along the discontinuity. Inset: Transducer layout used for seismic measurements.

maxima in transmitted wave amplitude (or as minima in the reflected wave amplitude), are measures of an impending reduction in the true contact area. This observation demonstrates that precursors and the associated increase in the rate of slip both indicate the loss of true contact area along the discontinuity.

In another set of experiments, we conducted direct shear experiments on limestone rock specimens obtained in Bedford, Indiana. Similar to the observations made on our gypsum specimens, the amplitude of the transmitted shear waves across the discontinuity increased upon the application of shear load and reached a peak prior to the peak shear strength of the discontinuity. The

precursors were identified as a maximum in the amplitude of the transmitted shear waves that occurred prior to the peak shear strength of the discontinuity, which were observed between -0.2 mm and -0.02 mm with respect to the macroscopic failure of the discontinuity and were observed between 60% and 96% of the peak displacement.

We used the displacement discontinuity model [Schoenberg, 1980; Pyrak-Nolte et al., 1990; Pyrak-Nolte, 1996; Hildyard et al., 2005; Choi, 2013] to estimate the change in fracture-specific stiffness during shearing. The displacement discontinuity model represents a discontinuity by a set of boundary conditions between two homogeneous, isotropic, linear elastic half-spaces. The boundary conditions assume continuous stresses but a discontinuity in displacements across the interface. The magnitude of the discontinuity in displacement is inversely proportional to the specific stiffness of the discontinuity (contact surface). Specific stiffness of the discontinuity has been shown to depend on the true contact area between the discontinuity surface and the aperture distribution of the void space in the discontinuity [Kendall and Tabor, 1971; Brown and Scholz, 1985, 1986; Hopkins et al., 1987; Pyrak-Nolte et al., 1990; Pyrak-Nolte, 1996; Cook, 1992] and to be related to fluid flow through a fracture through the deformed fracture topology [Petrovitch et al., 2013, 2014].

The displacement discontinuity model for waves propagated at normal incidence to the discontinuity [Pyrak-Nolte et al., 1990] yields transmission and reflection coefficients (equations (1) and (2)) that depend on the specific stiffness of the discontinuity, κ , the seismic impedance of the half-spaces, Z , given by the product of density and phase velocity and the frequency of the signal, ω .

$$T(\omega) = \frac{1}{1 - i\omega Z/2\kappa} \quad (1)$$

$$R(\omega) = \frac{-i\omega Z/2\kappa}{1 - i\omega Z/2\kappa} \quad (2)$$

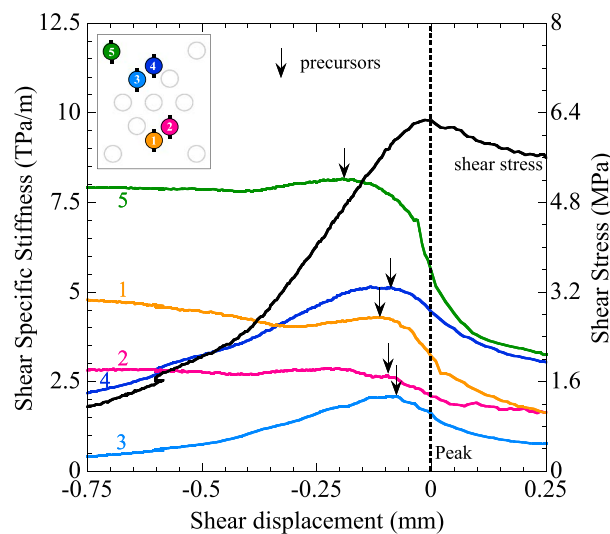


Figure 5. Shear specific stiffness variation during a shear experiment on an Indiana limestone specimen under an applied normal stress of 4 MPa. Inset: Transducer layout showing shear wave transducers oriented parallel to the shear direction.

Equations (1) and (2) are coupled to determine the specific stiffness of the

discontinuity by using the ratio of the measured transmitted (T) and reflected (R) wave amplitudes [Choi, 2013; Choi et al., 2014]:

$$\kappa_z(\omega) = \frac{\omega\rho V_p}{2} \left| \frac{T}{R} \right| \quad (3)$$

$$\kappa_x(\omega) = \frac{\omega\rho V_s}{2} \left| \frac{T}{R} \right| \quad (4)$$

where κ_z and κ_x are the discontinuity normal and shear-specific stiffnesses, respectively, $V_p = 4483$ m/s and $V_s = 2497$ m/s are the compressional and shear wave velocities for intact limestone, respectively, and $\rho = 2300$ kg/m³ is the density of limestone.

Figure 5 illustrates the variation in shear-specific stiffness during a shear experiment on a discontinuity in an Indiana limestone specimen. A maximum in the shear specific stiffness of the discontinuity occurred prior to the peak shear strength of the discontinuity and then decreased as slip occurred. The precursory peak was indicative of the impending failure of the discontinuity.

4. Conclusions

The most important implication of this study is the presence of ultrasonic precursors prior to the shear failure of frictional discontinuities in both gypsum, a rock model material, and Indiana limestone, a natural rock. Precursors can be identified as the maximum in transmitted wave amplitude or the minimum in the reflected wave amplitude. We observed ultrasonic precursors well before slip or failure occurred along the discontinuity. These precursors were associated with an acceleration of slip across the discontinuity and were attributable to a reduction in the discontinuity local shear stiffness. If the same physical mechanisms observed in our laboratory studies occur in nature, our data suggest that active seismic monitoring of discontinuities may provide a basis for earthquake prediction.

Acknowledgments

The data for this paper can be made available upon request from the author. This work was supported by the National Science Foundation, Geomechanics and Geotechnical Systems Program, under grant CMS-0856296 to Purdue University.

The Editor thanks two anonymous reviewers for their assistance in evaluating this paper.

References

- Aggarwal, Y. P., L. R. Sykes, J. Armbruster, and M. L. Sbar (1973), Premonitory changes in seismic velocities and prediction of earthquakes, *Nature*, *241*, 101–104, doi:10.1038/241101a0.
- Bobet, A., and H. H. Einstein (1998), Fracture coalescence in rock-type materials under uniaxial and biaxial compression, *Int. J. Rock Mech. Min. Sci.*, *35*, 863–888, doi:10.1016/S0148-9062(98)00005-9.
- Brace, W. F. (1972), Laboratory studies of stick-slip and their application to earthquakes, *Tectonophysics*, *14*, 189–200, doi:10.1016/0040-1951(72)90068-6.
- Brace, W. F., and J. D. Byerlee (1966), Stick-slip as a mechanism for earthquakes, *Science*, *153*, 990–992, doi:10.1126/science.153.3739.990.
- Brown, S. R., and C. H. Scholz (1985), Closure of random elastic surfaces in contact, *J. Geophys. Res.*, *90*, 5531–5545, doi:10.1029/JB090iB07p05531.
- Brown, S. R., and C. H. Scholz (1986), Closure of rock joints, *J. Geophys. Res.*, *91*, 4939–4948, doi:10.1029/JB091iB05p04939.
- Bruhn, R. L., and R. A. Schultz (1996), Geometry and slip distribution in normal fault systems: Implications for mechanics and fault-related hazards, *J. Geophys. Res.*, *101*, 3401–3412, doi:10.1029/95JB03253.
- Bürgmann, R., and D. D. Pollard (1994), Slip distributions on faults: Effects of stress gradients, inelastic deformation, heterogeneous host-rock stiffness, and fault interaction, *J. Struct. Geol.*, *16*, 1675–1690, doi:10.1016/0191-8141(94)90134-1.
- Byerlee, J. (1978), A review of rock mechanics studies in the United States pertinent to earthquake prediction, *Pure Appl. Geophys.*, *116*, 586–602, doi:10.1007/BF00876526.
- Byerlee, J. D. (1970), The mechanics of stick-slip, *Tectonophysics*, *9*(5), 475–486, doi:10.1016/0040-1951(70)90059-4.
- Byerlee, J. D., and W. F. Brace (1968), Stick slip, stable sliding, and earthquakes-effect of rock type, pressure, strain rate, and stiffness, *J. Geophys. Res.*, *73*, 6031–6037, doi:10.1029/JB073i018p06031.
- Byerlee, J. D., and R. Summers (1975), Stable sliding preceding stick-slip on fault surfaces in granite at high pressure, *Pure Appl. Geophys.*, *113*, 63–68, doi:10.1007/BF01592899.
- Chen, W. Y., C. W. Lovell, G. M. Haley, and L. J. Pyrak-Nolte (1993), Variation of shear-wave amplitude during frictional sliding, *Int. J. Rock Mech. Min. Sci. Geomech. Abstr.*, *30*, 779–784, doi:10.1016/0148-9062(93)90022-6.
- Choi, M. K. (2013), Characterization of fracture stiffness subjected to normal and shear stress, PhD thesis, School of Civil Engineering, Purdue Univ., West Lafayette, Ind.
- Choi, M.-K., L. J. Pyrak-Nolte, and A. Bobet (2014), The effect of surface roughness and mixed-mode loading on the stiffness ratio K_x/K_z for fractures, *Geophysics*, *79*(5), doi:10.1190/GEO2013-0438.1.
- Chu, T. C., W. F. Ranson, M. A. Sutton, and W. H. Peters (1985), Applications of digital-image-correlation techniques to experimental mechanics, *Exp. Mech.*, *25*, 232–244, doi:10.1007/BF02325092.
- Cicerone, R. D., J. E. Ebel, and J. A. Britton (2009), A systematic compilation of earthquake precursors, *Tectonophysics*, *476*, 371–396, doi:10.1016/j.tecto.2009.06.008.
- Cook, N. G. W. (1992), Natural joints in rock: Mechanical, hydraulic and seismic behavior and properties under normal stress, *Int. J. Rock Mech. Min. Sci.*, *29*(3), 198–223, doi:10.1016/0148-9062(92)93656-5.
- Dieterich, J. H. (1978a), Preseismic fault slip and earthquake prediction, *J. Geophys. Res.*, *83*, 3940–3948, doi:10.1029/JB083iB08p03940.
- Dieterich, J. H. (1978b), Time-dependent friction and the mechanics of stick-slip, *Pure Appl. Geophys.*, *116*, 790–806, doi:10.1007/BF00876539.

- Dieterich, J. H. (1979), Modeling of rock friction: 1. Experimental results and constitutive equations, *J. Geophys. Res.*, *84*, 2161–2168, doi:10.1029/JB084iB05p02161.
- Dieterich, J. H., and B. D. Kilgore (1994), Direct observation of frictional contacts: New insights for state-dependent properties, *Pure Appl. Geophys.*, *143*, 283–302, doi:10.1007/BF00874332.
- Einstein, H. H., and R. C. Hirschfeld (1973), Model studies on mechanics of jointed rock, *ASCE J. Geotech. Div.*, *99*, 229–248.
- Goebel, T. H. W., D. Schorlemmer, T. W. Becker, G. Dresen, and C. G. Sammis (2013), Acoustic emissions document stress changes over many seismic cycles in stick-slip experiments, *Geophys. Res. Lett.*, *40*, 2049–2054, doi:10.1002/grl.50507.
- Hedayat, A. (2013), Mechanical and geophysical characterization of damage in rocks, PhD thesis, School of Civil Engineering, Purdue Univ., West Lafayette, Ind.
- Hildyard, M. W., R. P. Young, D. S. Collins, and W. Pettitt (2005), Seismic wave propagation to diagnose the state of fracturing, *J. S. Afr. I. Min. Metall.*, *105*, 437–446.
- Hopkins, D. L., N. G. W. Cook, and L. R. Myer (1987), Fracture stiffness and aperture as a function of applied stress and contact geometry, paper presented at 28th U.S. Symposium on Rock Mechanics, Tucson, Ariz.
- Jaeger, J. C., N. G. W. Cook, and R. W. Zimmerman (2007), *Fundamentals of Rock Mechanics*, Wiley-Blackwell, London, U. K.
- Johnson, T. L., and C. H. Scholz (1976), Dynamic properties of stick-slip friction of rock, *J. Geophys. Res.*, *81*, 881–888, doi:10.1029/JB081i005p00881.
- Johnson, P. A., H. Savage, M. Knuth, J. Gombert, and C. Marone (2008), Effects of acoustic waves on stick-slip in granular media and implications for earthquakes, *Nature*, *451*, 57–60, doi:10.1038/nature06440.
- Johnson, P. A., B. Ferdowsi, B. M. Kaproth, M. Scuderi, M. Griffa, J. Carmeliet, R. A. Guyer, P. Y. Le Bas, D. T. Trugman, and C. Marone (2013), Acoustic emission and microslip precursors to stick-slip failure in sheared granular material, *Geophys. Res. Lett.*, *40*, 5627–5631, doi:10.1002/2013GL057848.
- Kaproth, B. M., and C. Marone (2013), Slow earthquakes, preseismic velocity changes, and the origin of slow frictional stick-slip, *Science*, *341*, 1229–1232, doi:10.1126/science.1239577.
- Kendall, K., and D. Tabor (1971), An ultrasonic study of the area of contact between stationary and sliding surfaces, *Proc. R. Soc. London A*, *323*, 321–340, doi:10.1098/rspa.1971.0108.
- Lockner, D. A. (1993), The role of acoustic emission in the study of rock fracture, *Int. J. Rock Mech. Min. Sci. Geomech.*, *30*(7), 883–99, doi:10.1016/0148-9062(93)90041-B.
- Lockner, D. A., and J. D. Byerlee (1986), Changes in complex resistivity during creep in granite, *Pure Appl. Geophys.*, *124*, 659–676, doi:10.1007/BF00879603.
- Lockner, D. A., J. B. Walsh, and J. D. Byerlee (1977), Changes in seismic velocity and attenuation during deformation of granite, *J. Geophys. Res.*, *82*, 5374–5378, doi:10.1029/JB082i033p05374.
- Mair, K., and J. F. Hazzard (2007), Nature of stress accommodation in sheared granular material: Insights from 3D numerical modeling, *Earth Planet. Sci. Lett.*, *259*, 469–485, doi:10.1016/j.epsl.2007.05.006.
- Marone, C. (1998), The effect of loading rate on static friction and the rate of fault healing during the earthquake cycle, *Nature*, *391*, 69–72, doi:10.1038/34157.
- Martel, S. J., and D. D. Pollard (1989), Mechanics of slip and fracture along small faults and simple strike-slip fault zones in granitic rock, *J. Geophys. Res.*, *94*, 9417–9428, doi:10.1029/JB094iB07p09417.
- McLaskey, G. C., A. M. Thomas, S. D. Glaser, and R. M. Nadeau (2012), Fault healing promotes high-frequency earthquakes in laboratory experiments and on natural faults, *Nature*, *491*, 101–104, doi:10.1038/nature11512.
- Meredith, P. G., I. G. Main, and C. Jones (1990), Temporal variations in seismicity during quasi-static and dynamic rock failure, *Tectonophysics*, *175*, 249–268, doi:10.1016/0040-1951(90)90141-T.
- Morrow, C., L. Q. Shi, and J. Byerlee (1981), Permeability and strength of San Andreas fault gouge under high pressure, *Geophys. Res. Lett.*, *8*, 325–329, doi:10.1029/GL008i004p00325.
- Mutlu, O., and A. Bobet (2006), Slip propagation along frictional discontinuities, *Int. J. Rock Mech. Min. Sci.*, *43*, 860–876, doi:10.1016/j.ijrmm.2005.11.012.
- Nasuno, S., A. Kudrolli, and J. P. Gollub (1997), Friction in granular layers: Hysteresis and precursors, *Phys. Rev. Lett.*, *79*, 949–952, doi:10.1103/PhysRevLett.79.949.
- Ohnaka, M., and Y. Kuwahara (1990), Characteristic features of local breakdown near a crack-tip in the transition zone from nucleation to unstable rupture during stick-slip shear failure, *Tectonophysics*, *175*, 197–220, doi:10.1016/0040-1951(90)90138.
- Okubo, P. G., and J. H. Dieterich (1984), Effects of physical fault properties on frictional instabilities produced on simulated faults, *J. Geophys. Res.*, *89*, 5817–5827, doi:10.1029/JB089iB07p05817.
- Pan, B., K. Qian, H. Xie, and A. Asundi (2009), Two-dimensional digital image correlation for in-plane displacement and strain measurement: A review, *Meas. Sci. Technol.*, *20*, 062001, doi:10.1088/0957-0233/20/6/062001.
- Petrovitch, C., L. J. Pyrak-Nolte, and D. D. Nolte (2013), Scaling of fluid flow versus fracture stiffness, *Geophys. Res. Lett.*, *40*, 2076–2080, doi:10.1002/grl.50479.
- Petrovitch, C. L., L. J. Pyrak-Nolte, and D. D. Nolte (2014), Combined scaling of fluid flow and seismic stiffness in single fractures, *Rock Mech. Rock Eng.*, doi:10.1007/s00603-014-0591-z.
- Pyrak-Nolte, L. J. (1996), The seismic response of fractures and the interrelations among fracture properties, *Int. J. Rock Mech. Min. Sci.*, *33*, 787–802, doi:10.1016/S0148-9062(96)00022-8.
- Pyrak-Nolte, L. J., L. R. Myer, and N. G. W. Cook (1990), Transmission of seismic waves across single natural fractures, *J. Geophys. Res.*, *95*, 8617–8638, doi:10.1029/JB095iB06p08617.
- Sammonds, P., and M. Ohnaka (1998), Evolution of microseismicity during frictional sliding, *Geophys. Res. Lett.*, *25*, 699–702, doi:10.1029/98GL00226.
- Schoenberg, M. (1980), Elastic wave behavior across linear slip interfaces, *J. Acoust. Soc. Am.*, *68*, 1516–1521, doi:10.1121/1.385077.
- Scholz, C. H. (1998), Earthquakes and friction laws, *Nature*, *391*, 37–42, doi:10.1038/34097.
- Scholz, C. H. (2002), *The Mechanics of Earthquakes and Faulting*, Cambridge Univ. Press, New York.
- Scholz, C. H., P. Molnar, and T. Johnson (1972), Detailed studies of frictional sliding of granite and implications for the earthquake mechanism, *J. Geophys. Res.*, *77*, 6392–6406, doi:10.1029/JB077i032p06392.
- Schreier, H., J. Orteu, and M. A. Sutton (2009), *Image Correlation for Shape, Motion and Deformation Measurements*, Springer, New York.
- Shen, B., O. Stephansson, H. H. Einstein, and B. Ghahreman (1995), Coalescence of fractures under shear stresses in experiments, *J. Geophys. Res.*, *100*, 5975–5990, doi:10.1029/95JB00040.
- Sobolev, G., H. Spetzler, A. Koltsov, and T. Chelidze (1993), An experimental study of triggered stick-slip, *Pure Appl. Geophys.*, *140*(1), 79–94, doi:10.1007/BF00876872.

- Stesky, R., W. Brace, D. Riley, and P. Y. Robin (1974), Friction in faulted rock at high temperature and pressure, *Tectonophysics*, *23*, 177–203, doi:10.1016/0040-1951(74)90119-X.
- Thompson, B. D., R. P. Young, and D. A. Lockner (2009), Premonitory acoustic emissions and stick-slip in natural and smooth-faulted Westerly granite, *J. Geophys. Res.*, *114*, B02205, doi:10.1029/2008JB005753.
- Weeks, J. D., and T. E. Tullis (1985), Frictional sliding of dolomite: A variation in constitutive behavior, *J. Geophys. Res.*, *90*, 7821–7826, doi:10.1029/JB090iB09p07821.
- Weeks, J., D. Lockner, and J. Byerlee (1978), Changes in b-values during movement on cut surfaces in granite, *B. Seismol. Soc. Am.*, *68*, 333–341.
- Yabe, Y., N. Kato, K. Yamamoto, and T. Hirasawa (2003), Effect of sliding rate on the activity of acoustic emission during stable sliding, *Pure Appl. Geophys.*, *160*, 1163–1189, doi:10.1007/s000240300000.
- Yanagidani, T., S. Ehara, O. Nishizawa, K. Kusunose, and M. Terada (1985), Localization of dilatancy in Ohshima granite under constant uniaxial stress, *J. Geophys. Res.*, *90*, 6840–6858, doi:10.1029/JB090iB08p06840.
- Zoback, M. D., and J. D. Byerlee (1975), The effect of cyclic differential stress on dilatancy in Westerly granite under uniaxial and triaxial conditions, *J. Geophys. Res.*, *80*, 752–755, doi:10.1029/JB080i005p00752.